Journal of Molecular Structure 1198 (2019) 126857

Contents lists available at ScienceDirect

Journal of Molecular Structure

journal homepage: http://www.elsevier.com/locate/molstruc

Synthesis, single crystal X-ray analysis, and vibrational spectral studies of ethyl 6-bromo-5-((5-bromopyrimidin-2-yl)oxy)-2-((2, 6-dimethylmorpholino)methyl)-1-methyl-1*H*-indole-3-carboxylate

Dali Luo [a, b], Lanlan Ma [a, b], Zhixu Zhou [a, b], Zhuyan Huang [a, b, *]

[a] School of Pharmaceutical Sciences, Guizhou University, Guiyang, 550025, China
[b] Guizhou Engineering Laboratory for Synthetic Drugs, Guiyang, 550025, China

ARTICLE INFO

Article history:
Received 13 April 2019
Received in revised form
25 July 2019
Accepted 27 July 2019
Available online 29 July 2019

Keywords:
Mecarbinate
Single crystal X-ray spectrum
DFT

ABSTRACT

A new mecarbinate derivative, ethyl 6-bromo-5-((5-bromopyrimidin-2-yl)oxy)-2-((2,6- dimethylmorpholino)methyl)-1-methyl-1*H*-indole-3-carboxylate (**1**), was synthesized, and single crystals were grown by the gradual evaporation of acetone under ambient conditions. The optimized molecular crystal structure was determined based on DFT calculations at the B3LYP/6311G (2 d, p) level. Experimental and theoretical studies on the structure of the titled compound are presented.

© 2019 Elsevier B.V. All rights reserved.

1. Introduction

Indole derivatives constitute a class of very important organic and chemical products. Mecarbinate, an indole derivative, has been extensively applied in chemical and pharmaceutical industries as an important intermediate of arbidol hydrochloride (and its 4-substituted derivatives) [1], which is an effective antiviral and immunomodulatory drug [2,3]. Mecarbinate derivatives have been receiving attention since the 1960s due to their biological activity [4,5]. For example, 5-hydroxy-1,2-dimethyl-6-fluoro-1*H*-indole-3-carboxylate hydrochlorides and ethyl 5-hydroxy-4-(dimethylaminomethyl)-1-methyl-6-pyidin-3-yl-2-(phenylsulfinylmethyl)-1*H*-indole-3-carboxylate have been reported to exhibit antiviral activity against hepatitis *C* virus (HCV) [6]. In addition, 1-benzyl-2-dimethylaminomethyl-3-carbethoxy-5-acetoxy-6- bromo indole hydrochloride exhibited anti-influenza activity in studies employing a mouse model for influenza pneumonia [7]. Roller et al. [8] reported that *N*-benzyl substituted analogs of the anti-inflammatory drug, indomethacin, and indomethacin-related *N*-benzyl indoleacetamide, exhibited multidrug resistance related-protein 1 (MRP-1) modulatory activities [9] and selective cyclooxygenase-2 (COX-2) inhibition [10]. Moreover, indomethacin is used for the treatment of periarthritis, rheumatoid arthritis, osteoarthrosis, gout, ankylosing spondylitis, musculoskeletal system diseases, inflammatory diseases of connective tissue, thrombophlebitis, and other diseases accompanied by inflammation [11]. Over the years, the extensive application of mecarbinate derivatives has driven researchers to synthesize new analogs of them [6,12].

In this study, we synthesized compound **1**, a new mecarbinate derivative, which included a pyrimidine ring and a morpholine ring. To the best of our knowledge, this compound has not been reported as far as its relevance is concerned. To further study the biological activity of the titled compound, this study fully explores the structural characterization of the compound. The structure of compound **1** was characterized by ^{1}H NMR, ^{13}C NMR, FT-IR, and MS. Furthermore, the crystal structure was determined by single-crystal X-ray diffraction analysis, and the geometric data were calculated using the Gaussian 09 program package based on density functional theory (DFT).

2. Experimental

2.1. General remarks

Mass spectra were recorded in ESI mode on an Agilent 1100 LC-MS instrument (Agilent Technologies, Palo Alto, CA, USA). ^{1}H NMR

* Corresponding author. School of Pharmaceutical Sciences, Guizhou University, Guiyang, 550025, China.
E-mail address: tthhzy@126.com (Z. Huang).

https://doi.org/10.1016/j.molstruc.2019.07.104
0022-2860/© 2019 Elsevier B.V. All rights reserved.

and ^{13}C NMR spectra were recorded on a Bruker ARX-400, 400 MHz spectrometer (Bruker Bioscience, Billerica, MA, USA) using TMS as an internal standard. The IR spectrum of the titled compound was recorded on a Bruker IFS-55V IR spectrometer (Bruker, Germany), in the region of 4000–400 cm^{-1} using the KBr pellet technique with 1.0 cm^{-1} resolution. The X-ray diffraction data of the crystal of **1** were recorded using a Bruker P4 X-diffractometer; the data were collected using a graphite-monochromated Mo Kα radiation (λ = 0.71073 Å) at 296 (2) K. For **1**, the data collection: APEX2; cell refinement: SAINT; the program used to solve structures: SHELXS-97; the program used to refine structures and draw molecular figures: SHELXTL-97; the program used to measure centroid-centroid distance: Mercury 2.3. All the materials were obtained from commercial suppliers and were used without further purification.

2.2. Experimental details

The synthesis route of compound **1** is shown in Scheme 1. The specific details are provided in Supplementary Information.

2.3. X-ray crystal structure determination

The title compound **1** was dissolved in acetone and the solvent was slowly evaporated under air at room temperature. A few days later, the title compound single crystal suitable for X-ray crystallographic analysis was obtained. A colorless transparent crystal having a size of 0.22 mm × 0.20 mm × 0.18 mm was selected to be mounted on the glass fiber in a random direction for data collection. X-Ray diffraction data of the title compound crystal were recorded with a Bruker P4 X-diffractometer and the data were collected by using graphite -monochromated Mo-$K\alpha$ radiation ($\lambda = 0.71073$ Å) at 296 (2) K. A total of 15607 reflections were collected in the range of 1.41–25.32° (index ranges: $14 \le h \le 18$, $-12 \le k \le 13$, $-16 \le l \le 17$) by using an φ-ω scan mode and 4346 were independent with $R_{int} = 0.0390$, of which 2724 observed reflections with $I > 2\sigma$ (I) were used in the structure determination and refinements. The structure was solved by direct methods with SHELXS-97 program [13]. Refinements were done by full-matrix least-squares on F^2 with SHELXL-97 [13]. The hydrogen atoms were determined with theoretical calculations.

2.4. Quantum chemistry/DFT calculation

The DFT calculations were performed in the ground state (in vacuo) with Gaussian 09 software packag [14] by using the B3LYP method with the 6-311G (2 d, p) basis set. The geometrical, electronic and energy parameters were extracted from Gaussian 09 program [15] based on the optimized structures.

3. Results and discussion

3.1. Conformational determination

The conformation of a molecule critically influences its physical and chemical properties [16,17]. Thus, reliable conformational analysis plays a key role in understanding the structure of a molecule. The initial conformational search of compound **1** was performed by the Spartan 08 program [18] with an MMFF [19,20] molecular mechanics force field. Subsequently, geometry optimizations and frequency calculation of all the possible conformers were performed at the DFT/B3LYP/6-311G** [21,22] level using the Gaussian 09 package [23]. From the relative free energies, the percentage population of each conformation in a room-temperature equilibrium mixture was predicted. The relative Gibbs free energies and Boltzmann distribution of **1** are shown in Table 1.

The relatively stable conformers of compound **1** are given in Fig. 1. For compound **1**, conformers **1**–**1** (38.01%), **1**–**2** (25.74%), **1**–**3** (22.19%), and **1**–**4** (14.06%) are significantly populated at room temperature.

Table 1
Gibbs free energies (G), relative Gibbs free energies (△G)[a] and Boltzmann weighting factor (P%)[b] of **1** conformers by using the DFT/B3LYP/6-311G (2 d, p) method.

Conformer	G (kcal mol^{-1})	△G (kcal mol^{-1})	*Pi*%
1–1	−4116613.84	0	38.01
1–2	−4116613.61	0.2284	25.74
1–3	−4116613.52	0.3156	22.19
1–4	−4116613.25	0.5829	14.06

[a] Which related to the most stable conformer.
[b] Boltzmann weighting factor (P_i%) based on △G.

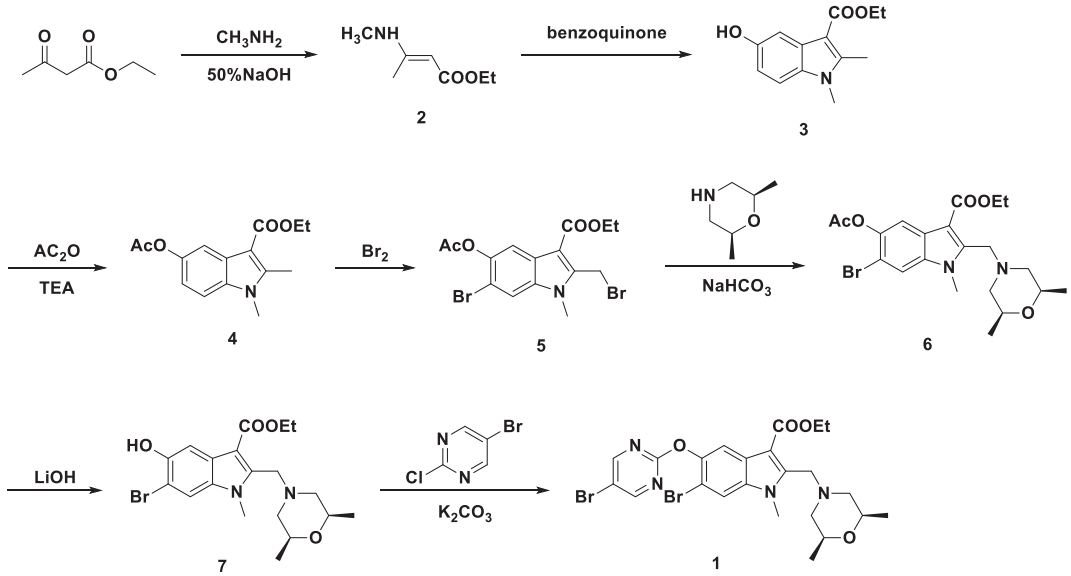

Scheme 1. Synthesis route of compound 1.

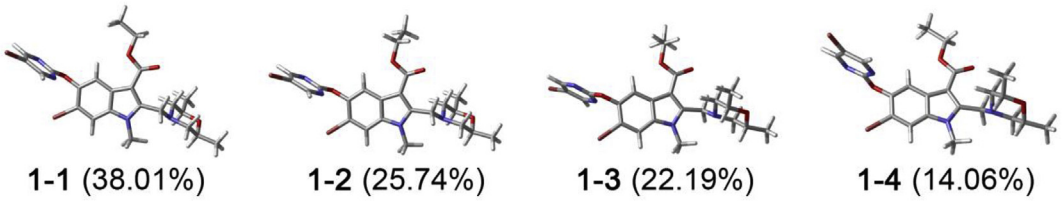

Fig. 1. Relatively stable conformers of **1**.

The differences between the four conformers were attributed to the orientation of the ester group. The ground-state energies of **1**–**1** and **1**–**2**, and **1**–**3** and **1**–**4** are similar and only a slight difference between the orientations of ethyl in the five-member heterocyclic group was observed.

To obtain in-depth insight into the structural characteristics of the designed analogs, an X-ray structure analysis of **1** was performed. The crystal of **1** was grown by the gradual evaporation of acetone under ambient conditions, and a suitable crystal was obtained for crystallographic analysis. The measured value showed that **1** has a monoclinic system with a P2 (1)/c space group [cell: $a = 15.2683$ (8) Å, $b = 11.6093$ (5) Å, $c = 14.3751$ (7) Å, $\alpha = 90.00°$, $\beta = 109.07°$, $\gamma = 90.00°$, $V = 2408.23$ Å^3, $Z = 4$, and $\mu = 3.403$ mm^{-1}].

The crystal structure of **1** was compared with the DFT-optimized structures. The conformer **1**–**4** calculated by DFT is consistent with the crystal conformation obtained by X-ray diffraction, as shown in Fig. 2.

The main crystallographic data are summarized in Table 2. Some geometric parameters of the experimental values of crystal **1** and the calculated values of conformer **1**–**4** are listed in Table 3. As expected, most of the calculated geometry parameters for compound **1** are close to the X-ray data.

The title compound hydrogen bond details are listed in Table 4. Furthermore, the intramolecular C (10)—H (10) … O (2), C (13)—H (13B)···N (4) and C (17)—H (17B)···O (3) as well as intermolecular C (1B)—H (1B)···O (3) and C (23)—H (23A) … N (2B) hydrogen bonds found in the title compound play a major role in stabilizing the molecule (Fig. 3C). In addition to the afore-described interactions, it is worth noting that the crystal packing is further stabilized by one weak π-π stacking interactions. The perpendicular distance was found with distances of two benzene rings of two molecules being 3.64 Å (Fig. 3B).

Table 2
Crystal data and parameters for structure refinement of the titled compound, $C_{23}H_{26}Br_2N_4O_4$.

Compound	(1)
CCDC	1487099
Molecular formula	$C_{23}H_{26}Br_2N_4O_4$
Molecular weight	582.03
Crystal system/Space group	Monoclinic, P2 (1)/c
a, b, c(Å)	15.2683(8), 11.6093(5), 14.3751(7)
α, β, γ (°)	90.00, 109.07, 90.00
V (Å^3)	2408.23
Z	4
D_{calc} (g cm^{-3})	1.606
μ (mm^{-1})	3.403
Radiation λ (Å)	0.71073
Ranges/indices (*h, k, l*)	−14, 18; −12, 13; −16, 17
θ limit (°)	2.25–21.02
Parameters	372
T, K	296 (2)
Crystal dimensions (mm)	0.22 × 0.20 x 0.18
Reflections measured	15607
Unique reflections	4346
Observed reflections ($I > 2\sigma(I)$)	2724
R_1, wR_2 ($I > 2\sigma(I)$)	0.048,0.167
Goodness of fit on F^2	0.960
Programs	SHELX97

3.2. Molecular electrostatic potential(MEP)

To gain information on the region in which conformer **1**–**4** (the major conformer) undergoes intermolecular interactions, the molecular electrostatic potential was investigated by the B3LYP/6311G (2 d, p) method. In the MEP map, the different electrostatic potentials at the surface are represented by different colors, and the potential increases in the order of red < orange < yellow < green < blue. The color code of the maps in the range −6.0 e^{-2} (deepest red) to 6.0 e^{-2} (deepest blue) in title molecule surface, where red color denotes the electron rich area and blue region indicates electron deficient region. As shown in Fig. 4, the N2 atom in pyrimidine of the conformer **1**–**4** is surrounded by negative charges, indicating some possible nucleophilic attack sites. In addition, the positive charge regions are located on the H atom of the C13 atom.

3.3. Frontier molecular orbitals

Frontier molecular orbitals investigation frequently shows

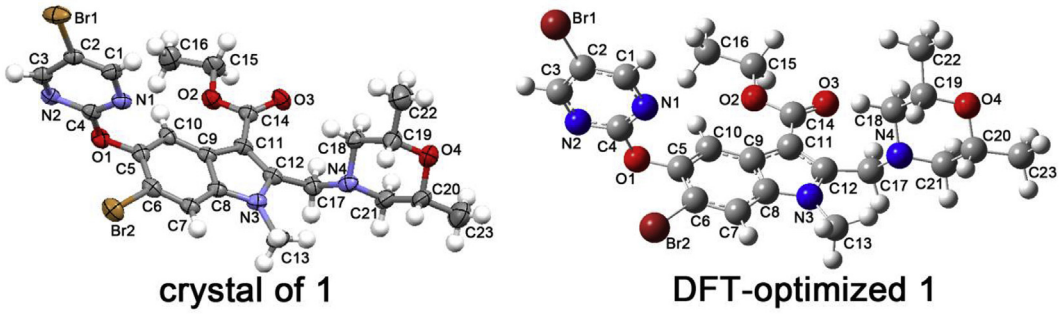

Fig. 2. DFT-optimized and crystal structures of **1**.

Table 3
Selected experimental and calculated geometry parameters for **1**.

Bond Distances (Å)	Exp.[a]	Calcd.[b]	Difference	Bond Distances (Å)	Exp.[a]	Calcd.[b]	Difference
Br (2)—C (6)	1.893	1.914	0.021	C (5)—O (1)	1.385	1.395	0.010
N (1A)-C (4A)	1.294	1.328	0.034	C (8)—N (3)	1.374	1.384	0.010
N (1A)-C (1A)	1.321	1.334	0.013	C (12)—N (3)	1.386	1.373	−0.013
C (1A)-C (2A)	1.323	1.389	0.066	C (13)—N (3)	1.467	1.459	−0.008
C (2A)-C (3A)	1.429	1.393	−0.036	C (14)—O (3)	1.218	1.218	0.000
C (2A)-Br (1A)	1.888	1.905	0.017	C (14)—O (2)	1.331	1.353	0.022
C (3A)-N (2A)	1.359	1.330	−0.029	C (15)—O (2)	1.469	1.450	−0.019
N (2A)-C (4A)	1.422	1.333	−0.089	C (17)—N (4)	1.472	1.472	0.000
C (4A)-O (1)	1.374	1.354	−0.020	C (18)—N (4)	1.477	1.468	−0.009
C (20)—C (23)	1.470	1.520	0.050	C (18)—C (19)	1.543	1.528	−0.015
C (20)—C (21)	1.510	1.529	0.019	C (19)—O (4)	1.429	1.433	0.004
C (21)—N (4)	1.445	1.466	0.021	C (19)—C (22)	1.499	1.519	0.020
C (5)—C (6)	1.414	1.407	−0.007	C (20)—O (4)	1.465	1.431	−0.034
Bond angle [°]	**Exp.[a]**	**Calcd.[b]**	**Difference**	**Bond angle [°]**	**Exp.[a]**	**Calcd.[b]**	**Difference**
C (4)-N (1)-C (1)	114.8	116.251	1.5	O (3)-C (14)-O (2)	122.4	122.069	−0.3
N (1A)-C (1A)-C (2A)	121.4	121.384	0.0	O (3)-C (14)-C (11)	125.2	126.231	1.0
C (1A)-C (2A)-C (3A)	118.0	117.332	−0.7	O (2)-C (14)-C (11)	112.4	111.699	−0.7
C (1A)-C (2A)-Br (1A)	124.6	121.390	−3.2	O (2)-C (15)-C (16)	105.2	107.601	2.4
C (3A)-C (2A)-Br (1A)	117.2	121.277	4.1	N (4)-C (17)-C (12)	111.8	112.849	1.0
N (2A)-C (3A)-C (2A)	122.7	121.669	−1.0	N (4)-C (18)-C (19)	106.7	110.161	3.5
C (3A)-N (2A)-C (4A)	103.7	115.941	12.2	O (4)-C (19)-C (22)	109.9	107.278	−2.6
N (1A)-C (4A)-O (1)	118.0	119.194	1.2	O (4)-C (19)-C (18)	109.5	110.060	0.6
N (1A)-C (4A)-N (2A)	133.0	127.420	−5.6	C (22)-C (19)-C (18)	110.2	112.794	2.6
O (1)-C (4A)-N (2A)	107.4	113.385	6.0	O (4)-C (20)-C (23)	108.6	107.298	−1.3
C (10)-C (5)-O (1)	118.5	118.452	0.0	O (4)-C (20)-C (21)	108.3	110.172	1.9
O (1)-C (5)-C (6)	119.6	120.130	0.5	C (23)-C (20)-C (21)	111.7	112.798	1.1
C (4A)-O (1)-C (5)	116.0	119.494	3.5	N (4)-C (21)-C (20)	110.2	110.317	0.1
C (14)-O (2)-C (15)	115.9	116.428	0.5	C (8)-N (3)-C (12)	109.5	109.282	−0.2
N (3)-C (8)-C (7)	129.0	129.167	0.2	C (8)-N (3)-C (13)	125.0	124.425	−0.6
N (3)-C (8)-C (9)	108.3	108.202	−0.1	C (12)-N (3)-C (13)	125.5	126.222	0.7
C (10)-C (9)-C (11)	134.8	135.013	0.2	C (21)-N (4)-C (17)	109.3	111.043	1.7
C (11)-C (12)-N (3)	108.3	109.239	0.9	C (21)-N (4)-C (18)	109.8	110.028	0.2
C (11)-C (12)-C (17)	130.3	129.685	−0.6	C (17)-N (4)-C (18)	110.8	112.490	1.7
N (3)-C (12)-C (17)	120.8	121.049	0.2	C (19)-O (4)-C (20)	110.0	112.659	2.7

[a] Experimental geometry parameters for molecule **1**.
[b] Calculated geometry parameters for conformer **1**—**4**.

Table 4
Hydrogen bonds for the title compound (Å, °).

D—H … A	*d* (D—H)	*d* (H···A)	*d* (D···A)	∠DHA
C (1B)—H (1B)···O (3)^{i}	0.93	2.50	3.270 (19)	140
C (10)—H (10) … O (2)	0.93	2.54	3.015 (8)	112
C (13)—H (13B)···N (4)	0.96	2.45	3.155 (10)	130
C (17)—H (17B)···O (3)	0.97	2.46	3.116 (8)	125
C (23)—H (23A) … N (2B)^{ii}	0.96	2.44	3.30 (2)	150

Symmetry code: (i) -x, 1/2 + y, 3/2 - z; (ii) 1 + x, y, z.

important in reactive prediction [24,25]. The highest occupied molecular orbital (HOMO), which is regarded as an electrons donor, is related to potential electron delocalization directly. The energy of HOMO reveals ability of charges transfer. On the other hand, the lowest unoccupied molecular orbital (LUMO) describes an area where electrons can be accepted, and the energy of LUMO is regarded as electron affinity [26]. The energy of band gap expresses the energy difference between this two important FMOs which signifies the stability of molecular structure.

To investigate the chemical stability of conformer **1**—**4**, the energies of the highest occupied molecular orbital (HOMO), the lowest unoccupied molecular orbital (LUMO), and their orbital energy gap were calculated by the B3LYP/6-311G (2 d, p) method. The pictorial illustration of the frontier molecular orbitals (FMOs) and their respective positive and negative regions represented by red and green colors are shown in Fig. 5. The values of LUMO and HOMO were −1.7943 eV and −6.1631 eV, respectively. The value of the energy separation between the HOMO and LUMO

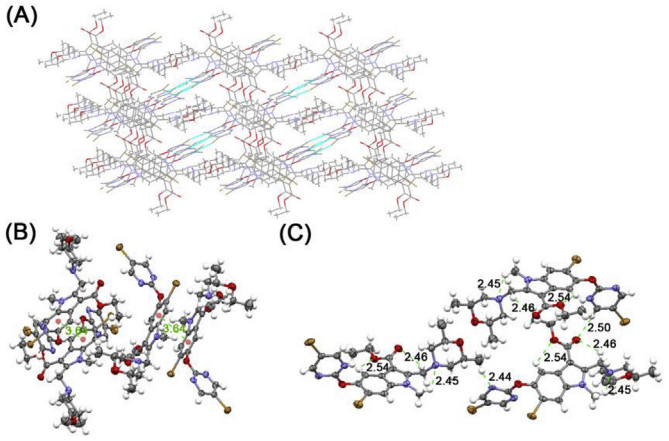

Fig. 3. (A) The crystal packing of title compound; (B) π-π stacking of compound **1** and centroid—centroid distances between two molecules; (C) The distance of the hydrogen bond of the title compound.

was −4.3688 eV for conformer **1**—**4**. The large HOMO—LUMO gap automatically implied high excitation energies of the excited states and good stability. Furthermore, the ionization energyand electron affinity can be expressed as: $I = -E_{HOMO} = 6.1631$ eV, $A = -E_{LUMO} = 1.7943$ eV. The hardness, which can be denoted as: $\eta = (I-A)/2$, indicates the resistance toward the deformation of the electron cloud of chemical systems under small perturbation

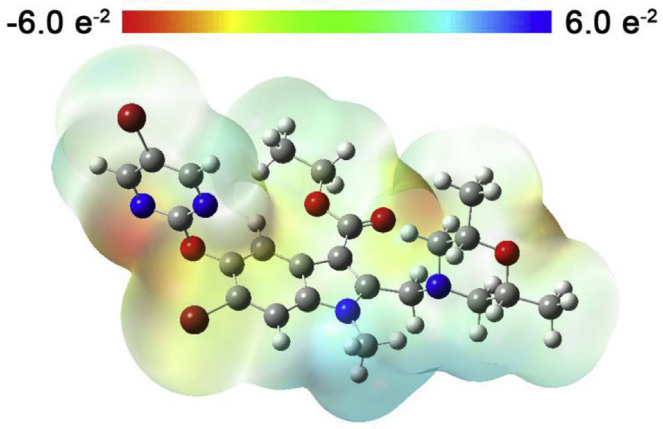

Fig. 4. Molecular electrostatic potential map of conformer **1**–**4**.

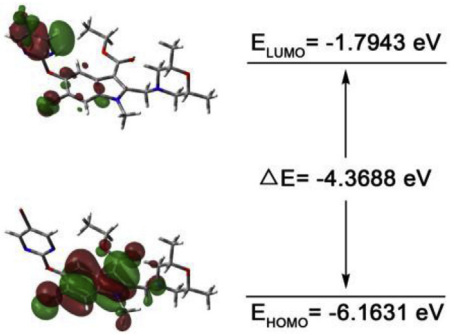

Fig. 5. The highest occupied and lowest unoccupied molecular orbitals of conformer **1**–**4** obtained by the DFT/6311G (2 d, p) method.

encountered during chemical process [27–29]. The hardness of compound **1** is 2.1844 eV.

3.4. Vibrational analysis

3.4.1. Carboxylate group (−COO−) vibrations

For the primary ester groups, the stretching deformation vibration is generally indicated by a sharp absorption peak in the region around 1735 cm^{-1} ($V_{C=O}$) and two or three strong correlation absorption bands in the region between 1300 and 1050 cm^{-1} (V_{C-O-C}). The frequency band indicative of C=O shifts to the right if the carbonyl group in the ester group is conjugated to the aromatic ring. Thus, the stretching vibration of C=O is indicated by a very strong band at 1688 cm^{-1}, as showed in Supporting Information. This band is attributed to the relatively strong conjugation effects of the indole ring, and the absorption bands at 1688 cm^{-1} were assigned to the asymmetrical stretching mode of C=O in molecule **1**.

3.4.2. Ether (C−O−C) vibrations

The C−O−C stretching vibrations are expected within the region of 1270–1010 cm^{-1}. Both the asymmetric stretching vibration frequency and the symmetric stretching peak intensity increase when the oxygen atom of ether oxy is connected to the aromatic ring or alkenyl group. There are two kinds of ethers positioned at different chemical locations in the title molecule. One is an aromatic oxide and its asymmetrical stretching vibration and symmetrical stretching vibration frequencies are 1238 cm^{-1} and 1036 cm^{-1}, respectively, since the ether group is connected to the pyrimidine ring and the indole ring, which can be explained by the resonance effect. In addition, according to the above analysis, the vibrational frequencies observed at 1113 cm^{-1} in the IR spectrum are assigned to the stretching vibrations of the ether, which is located in the morpholine ring.

3.4.3. C−Br vibrations

The vibration belonging to the C−Br bond, through which the halogen atom and the ring are linked, is indicated since it is possible that the vibrations are mixed due to the lowering of the molecular symmetry and the presence of heavy atoms [30–32]. In the organic halogen compounds, the bands at 1360–1000 cm^{-1}, 760–505 cm^{-1}, and 650–485 cm^{-1} may be assigned to the C−F, C−Cl, and C−Br stretching vibrations, respectively [33]. In our discussion, a shift in the absorption frequencies of C−Br may occur owing to the vibrational coupling with neighboring C groups. The strong IR bands obtained at 710 cm^{-1} and 604 cm^{-1} for $C_{30}Br_{33}$ and C_2Br_{25}, respectively, may be attributed to the stretching vibrations of C−Br.

3.4.4. C=C vibrations

The peaks at approximately 1600 cm^{-1} and 1500 cm^{-1} are the characteristic absorption bands of the stretching vibrations of the aromatic ring skeleton. In compound **1**, one of the C=C stretching vibrations of the aromatic ring overlaps with the vibrations of the C=O stretching mode. The bands at 1560 cm^{-1} and 1550 cm^{-1} may be assigned to the stretching vibrations of C=C. Moreover, the C=N stretching vibrational bands, which are too weak to be identified except in the presence of other substituent groups in the IR spectrum, usually coincides with the C=C vibrational bands in the region of 1690–1590 cm^{-1}. Consequently, it is not discussed herein.

3.4.5. −CH group vibrations

The aromatic C−H stretching vibrations in the substituted benzene rings are generally indicated by the bands in the high region of 3000–3100 cm^{-1} [34,35]. As shown in Fig. S2, the weak band at 3054 cm^{-1} in the IR spectrum can be assigned to the C−H stretching modes of the pyrimidine ring. For this compound, the bands due to the C−H stretching modes of the benzene ring were observed at 3451 cm^{-1}.

3.4.6. −CH_2 group vibrations

Compound **1** has four CH_2 groups with sp^3 hybridization. Here, the bands indicative of the asymmetric stretching and scissoring vibration of the methylene group are expected in the regions of 2940–2915 cm^{-1} and 1385–1345 cm^{-1}, respectively [36]. In addition, the average peak at 2936 cm^{-1} in the IR spectrum is attributed to the asymmetric stretching vibration mode of CH_2(C15), while the strong bands at 1479 cm^{-1} indicate the scissoring vibrations of CH_2(C17), CH_2(C18), and CH_2(C21).

3.4.7. −CH_3 group vibrations

Compound **1** has three CH_3 groups. The bands, indicative of the methyl (−CH_3) symmetric stretching frequencies, appear in the region of 2885–2860 cm^{-1}, whereas those of the asymmetric stretching frequencies lie in the range of 2975–2950 cm^{-1} [37]. In Fig. S2, the bands at 2970 cm^{-1} and 2876 cm^{-1} are assigned to the asymmetric stretching vibration and symmetric stretching vibration of CH_3, respectively. Two strong and sharp peaks indicative of the asymmetrical deformation vibration and symmetrical deformation vibration are observed at 1445 cm^{-1} and 1373 cm^{-1}, respectively.

4. Conclusion

In this study, a mecarbinate derivative, ethyl 6-bromo-5-((5-bromopyrimidin-2-yl)oxy) -2-((2,6-dimethylmorpholino)methyl)-1-methyl-1*H*-indole-3-carboxylate, was synthesized by a 7-step reaction. Subsequently, the optimized structures of the molecule were determined based on DFT calculations by the B3LYP method with the 6-311 + G (2 d, p) basis set. The structures optimized by the DFT method were compared with those determined by X-ray diffraction studies. The results show that the crystal structures determined by single crystal X-ray diffraction and DFT calculations are very similarity.

Acknowledgement

This work was supported by the Science and Technology Program of Guizhou province ([2017]1049) and the Science and Technology Cooperation Program of Guizhou province (LH20167442). The theoretical calculations were conducted on the ScGrid and Deepcomp7000 the Supercomputing Center, Computer Network Information Center of Chinese Academy of Sciences.

Appendix A. Supplementary data

Supplementary data to this article can be found online at https://doi.org/10.1016/j.molstruc.2019.07.104.

References

[1] P. Gong, F. Qin, L. Fang, D. Wang, D.-S. Yu, Synthesis and in vitro antiviral activities of some new 2-arylthiomethyl-4-tertiaryaminomethylsubstituted derivatives of 6-bromo-3-ethoxycarbonyl-5-hydroxy indoles, Chin. Chem. Lett. 15 (1) (2004) 19–22.
[2] Q. Liu, H.-R. Xiong, L. Lu, Y.-Y. Liu, F. Luo, W. Hou, Z.-Q. Yang, Antiviral and anti-inflammatory activity of arbidol hydrochloride in influenza A (H1N1) virus infection, Acta Pharmacol. Sin. 34 (8) (2013) 1075–1083.
[3] R.G. Glushkov, T.A. Gus'kova Arbidol, A new domestic immunomodulant, Pharm. Chem. J. 33 (3) (1999) 115–122.
[4] S.A. Zotova, V.I. Shvedov, Synthesis and some pharmacological properties of derivatives of indole and benzofuran containing the imidazole pharmacophore, Pharm. Chem. J. 28 (2) (1994) 103–106.
[5] F.A. Trofimov, N.G. Tsyshkova, V.I. Nozdrich, A.N. Grinev, Investigation in the field of quinones, Pharm. Chem. J. 5 (1) (1971) 27–28.
[6] A.V. Ivashchenko, P.M. Yamanushkin, O.D. Mit'Kin, V.M. Kisi, O.M. Korzinov, V.Yu Vedenskii, I.A. Leneva, E.A. Bulanova, V.V. Bychko, I.M. Okun, Synthesis and antiviral activity of ethyl 1,2-dimethy l-5-hydroxy-1*H*-Indole-3-carboxylates and their derivatives, Pharm. Chem. J. 47 (12) (2014) 636–650.
[7] A.N. Grinev, E.K. Panisheva, A.A. Cherkasova, A.N. Fomina, I.S. Nikolaeva, E.A. Golovanova, M.G. ll'ina, Synthesis and antiviral activity of 2-alkylaminomethyl derivatives of 5-oxyindole, Pharm. Chem. J. 21 (1) (1987) 48–51.
[8] A. Roller, O.R. Bähr, J. Streffer, S. Winter, M. Heneka, M. Deininger, R. Meyermann, U. Naumann, E. Gulbins, M. Weller, Selective potentiation of drug cytotoxicity by NSAID in human glioma cells: the role of COX-1 and MRP, Biochem. Biophys. Res. Commun. 259 (3) (1999) 60–65.
[9] A.R. Maguire, S.J. Plunkett, S. Papota, M. Clynesb, R. O'Connorb, S. Touheyb, Synthesis of indomethacin analogues for evaluation as modulators of MRP activity, Bioorg. Med. Chem. 9 (3) (2001) 745–762.
[10] Y. Leblanc, W.C. Black, C.C. Chan, S. Charleson, D. Delorme, D. Denis, Synthesis and biological evaluation of both enantiomers of L-761,000 as inhibitors of cyclooxygenase 1 and 2, Bioorg. Med. Chem. Lett 6 (6) (1996) 731–736.
[11] A.V. Ivachtchenko, P.M. Yamanushkin, O.D. Mitkin, O.I. Kiselev Bromination of indomethacin, Mendeleev Commun. 20 (20) (2010) 111–112.
[12] A.V. Ivashchenko, P.M. Yamanushkin, O.D. Mit'Kin, I.A. Leneva, I.T. Fedyakina, Synthesis and antiviral activity of functionally substituted indole-3-acetic acids, Pharm. Chem. J. 45 (5) (2011) 261–266.
[13] Y. Lin, Z.Y. Li, M. Zhang, X.Y. Yuan, Synthesis, crystal structure and anti-fungal activity of 2-(4-chloro phenyl)-1,3-dimethyl-2,3-dihydro-1*H*-perimidine, Chin. J. Struc. Chem. 35 (8) (2016) 1181–1185.
[14] J.G. Malecki, Synthesis, crystal, molecular and electronic structures of thiocyanate hydrido-carbonyl ruthenium(II) complexes with imidazole derivatives ligands, Polyhedron 29 (12) (2010) 2489–2497.
[15] M. Grabda, S. Oleszek-Kudlak, E. Shibata, T. Nakamur, Gas phase thermodynamic properties of PBDEs, PBBs, PBPs, HBCD and TBBPA predicted using DFT method, J. Mol. Struct. Theochem. 822 (1) (2007) 38–44.
[16] T. Mori, Y. Inoue, S. Grimme, Time dependent density functional theory calculations for electronic circular dichroism spectra and optical rotations of conformationally flexible chiral donor-acceptor dyad, J. Org. Chem. 71 (26) (2006) 9797–9806.
[17] D. Marchesan, S. Coriani, C. Forzato, P. Nitti, G. Pitacco, K. Ruud, Optical rotation calculation of a highly flexible molecule: the case of paraconic acid, J. Phys. Chem. A 109 (7) (2005) 1449–1453.
[18] M. Kwit, N.D. Sharma, D.R. Boyd, J. Gawronski, Determination of absolute configuration of conformationally flexible cis-dihydrodiol metabolites: effect of diene substitution pattern on the circular dichroism spectra and optical rotations, Chirality 20 (5) (2010) 609–620.
[19] B. Altava, M.I. Burguete, N. Carbó, S.V. Luis, V. Martí-Centelles, C. Vicen, Bis(amino amides) derived from natural amino acids as chiral receptors for N-protected dicarboxylic amino acids, Tetrahedron Lett. 54 (1) (2013) 72–79.
[20] N. Huang, C. Kalyanaraman, K. Bernacki, M.P. Jacobson, Molecular mechanics methods for predicting protein-ligand binding, Phys. Chem. Chem. Phys. 8 (44) (2006) 5166–5177.
[21] W. Koch, M.C. Holthausen, Chapter 1. Elementary quantum chemistry, Pharm. Chem. J. 3 (52) (2001) 30–37.
[22] P. Geerlings, F.D. Proft, W. Langenaeker, Conceptual density functional theory, Chem. Rev. 103 (5) (2003) 1793–1873.
[23] G.-Y.J. Im, S.M. Bronner, A.E. Goetz, R.S. Paton, P.H.-Y. Cheong, K.N. Houk, N.K. Garg, Indolyne experimental and computational studies: synthetic applications and origins of selectivities of nucleophilic additions, J. Am. Chem. Soc. 132 (50) (2010) 17933–17944.
[24] K. Fukui, T. Yonezawa, H. Shingu, A molecular orbital theory of reactivity in aromatic hydrocarbons, J. Chem. Phys. 20 (10) (2004), 1653-1653.
[25] M.D. Rozeboom, I.M. Tegmo-Larsson, K. Houk, Frontier molecular orbital theory of substituents effects on regioselectivities of nucleophilic additions and cycloadditions to benzoquinones and naphthoquinones, J. Org. Chem. 46 (11) (1981) 2338–2345.
[26] C.-G. Zhan, J.A. Nichols, D.A. Dixon, Ionization potential, electron affinity, electronegativity, hardness, and electron excitation energy? Molecular properties from density functional theory orbital energies, J. Phys. Chem. A 107 (20) (2003) 4184–4195.
[27] R.G. Parr, R.G. Pearson, Absolute hardness: companion parameter to absolute electronegativity, J. Am. Chem. Soc. 15 (13) (1984) 7512–7516.
[28] R.G. Pearson, Absolute electronegativity and hardness correlated with molecular orbital theory, Proc. Natl. Acad. Sci. 83 (22) (1986) 8440–8441.
[29] R.G. Parr, P.K. Chattaraj, Chattaraj, K. Pratim, Principle of maximum hardness, J. Am. Chem. Soc. 113 (5) (1991) 1854–1855.
[30] V.S. Madhavan, H.T. Varghese, S. Mathew, J. Vinsova, C.Y. Panicker, FT-IR, FT-Raman and DFT calculations of 4-chloro-2-(3,4-dichlorophenylcarbamoyl) phenyl acetate, Spectrochim. Acta Part A Molecular & Biomolecular Spectroscopy 72 (3) (2009) 547–553.
[31] C.S. Hiremath, J. Yenagi, J. Tonannavar, FT-Raman and infrared spectra and vibrational assignments for 3-chloro-4-methoxybenzaldehyde, as supported by ab initio, hybrid density functional theory and normal coordinate calculations, Spectrochim. Acta A Mol. Biomol. Spectrosc. 68 (3) (2007) 710–717.
[32] V. Sortur, J. Yenagi, J. Tonannavar, V.B. Jadhav, M.V. Kulkarni, Vibrational assignments for 7-methyl-4- bromomethylcoumarin, as aided by RHF and B3LYP/6-31G* calculations, Spectrochim. Acta Part A Molecular & Biomolecular Spectroscopy 71 (2) (2009) 688–694.
[33] D.A. Long, Infrared and Raman characteristic group frequencies, Tables and charts george socrates John Wiley and Sons, Ltd, chichester, third edition, J. Raman Spectrosc. 35 (10) (2010), 905-905.
[34] V. Krishnakumar, X.R. John, Molecular and vibrational structure of 2-mercapto pyrimidine and 2,4-diamino -6-hydroxy-5-nitroso pyrimidine: FT-IR, FT-Raman and quantum chemical calculations, Spectrochim. Acta Part A Molecular & Biomolecular Spectroscopy 63 (2) (2006) 454–463.
[35] M.A. Iramain, A.E. Ledesma, S.A. Brandán, Structural properties and vibrational analysis of Potassium 5-Br-2-isonicotinoyltrifluoroborate salt. Effect of Br on the isonicotinoyl ring, J. Mol. Struct. 1184 (2019) 146–156.
[36] M. Minteguiaga, E. Dellacassa, M.A. Iramain, C.A.N. Catalan, S.A. Brandan, FT-IR, FT-Raman, UV-Vis, NMR and structural studies of Carquejyl Acetate, a component of the essential oil from Baccharis trimera (Less.) DC. (Asteraceae), J. Mol. Struct. 1177 (2019) 499–510.
[37] M. Minteguiaga, E. Dellacassa, M.A. Iramain, C.A.N. Catalan, S.A. Brandan, Synthesis, Spectroscopic characterization and structural study of carquejiphenol, a 2-Isopropenyl-3-methylphenol derivative with potential medicinal uses, J. Mol. Struct. 1165 (2018) 332–343.